UNIVERSITY OF CALIFORNIA SAN DIEGO

Promyelocyte HL-60 Cell-line Demonstrates the Involvement of NETosis-Related Proteins in Neutrophil Nuclear Morphology Dynamics

A Thesis submitted in partial satisfaction of the requirements for the degree Master of Science

in

Biology

by

Laura Marie Waters

Committee in charge:

Professor Cornelis Murre, Chair
Professor Matthew Daugherty
Professor Yang Xu

2018

The Thesis of Laura Marie Waters is approved, and it is acceptable in quality and form for publication on microfilm and electronically:

_____

_____

_____
Chair

University of California San Diego

2018

DEDICATION

This Thesis is dedicated to my parents, Dan and Jocelyn Waters, for their never-ending support. Without their love and dedication to helping me reach my full potential, this Thesis and all the work leading up to it would not be possible.

TABLE OF CONTENTS

LIST OF ABBREVIATIONS

Abbreviation	Explanation
ABAH	4-Aminobenzoic Hydrazide
ATRA	All-Trans Retinoic Acid
CGD	Chronic Granulomatous Disease
CTCF	CCCTC-Binding Factor
CXCR	C-X-C Motif Chemokine Receptor
DAG	Diacylglycerol
DAPI	4′,6-Diamidino-2-Phenylindole
dHL-60	Differentiated HL-60
DMF	Dimethylformamide
DPBS	Dulbecco's Phosphate Buffered Saline
DPI	Diphenyleneiodonium Chloride
IF	Immunofluorescent
IL8	Interleukin 8
LBR	LaminB1 Receptor
MPO	Myeloperoxidase
NADPH	Nicotinamide Adenine Dinucleotide Phosphate
NE	Neutrophil Elastase
NEi	GW311616A
NET	Neutrophil Extracellular Trap
NOX	Nicotinamide Adenine Dinucleotide Phosphate Oxidase
PAD4	Peptidylarginine Deiminase 4
PBS	Phosphate Buffered Saline
PKC	Protein Kinase C
PMA	Phorbol 12-Myristate 13-Acetate

PRR	Pattern-Recognition Receptor
ROS	Reactive Oxygen Species
TAD	Topologically Associated Domain
US	Unstimulated

LIST OF FIGURES

ACKNOWLEGDEMENTS

I would like to acknowledge Distinguished Professor Cornelis Murre for his guidance as my committee chair. He gave me the opportunities I needed to accomplish this research, as well as his support in my work and academic development.

Additionally, I would like to acknowledge Postdoctoral Researcher Matthew Denholtz for his tremendous help in the planning and editing of this thesis. He has been teaching me from the very start of my work in the lab, and his guidance was essential for both the creation of this thesis and the execution of this research.

ABSTRACT OF THE THESIS

Promyelocyte HL-60 Cell-line Demonstrates the Involvement of NETosis-Related Proteins in Neutrophil Nuclear Morphology Dynamics

by

Laura Marie Waters

Master of Science in Biology

University of California San Diego, 2018

Professor Cornelis Murre, Chair

Neutrophils are characterized by a unique nuclear morphology, where the nucleus possesses a segmented multi-lobed form. During inflammation, neutrophils become activated and utilize their anti-microbial abilities. Neutrophil activation and extracellular trap formation are associated with the cell undergoing a change in nuclear morphology via delobing of the nucleus. While much work has been done concerning which parts of the activation pathway are required for NETosis, little is known about which portions of the activation pathway are involved with these morphology dynamics. Using quantitative image analysis, we established the promyelocyte HL-60 cell-line as a model system in which to study human

neutrophil nuclear morphology dynamics and differentiated HL-60s as a model to investigate activation-induced nuclear morphological changes. We find that ATRA differentiated HL-60s and DMF differentiated HL-60s can be used to observe changes in the measured circularity of the nucleus induced by PMA and A23187 stimulation respectively. Using chemical inhibitors in differentiated HL-60 stimulation, it was discovered that NOX and NE activity are required for PMA-induced nuclear morphological change while MPO and PAD4 activity are not, and that PAD4 activity is required for A23187-induced nuclear morphological change. These findings demonstrate how factors that are known to contribute to NETosis also contribute to pre-NETosis neutrophil nuclear dynamics.

INTRODUCTION

Neutrophils are innate immune cells that play an integral role as the first line of defense against invading pathogens. Patients with neutrophil deficiencies are prone to contracting major infections and, alternatively, misregulation of neutrophil activity is associated with autoimmune disease (1, 2). Neutrophils utilize multiple distinct mechanisms for defense against infections that are triggered in response to distinct pathogens or inflammatory stimuli. Together these facts showcase how neutrophils are an important aspect of the human immune system. Furthering our understanding of the mechanisms behind neutrophil activity is thus relevant to human health.

Neutrophils are produced in the bone marrow through granulopoiesis. This process involves three sequential pools of different cell types starting with hematopoietic stem cells (HSCs). HSCs differentiate into lymphoid-primed multipotent progenitor cells, which can subsequently differentiate into granulocyte-monocyte progenitor (GMP) cells. GMPs then differentiate into cell types of the mitotic pool of committed granulocytic progenitor cells still undergoing proliferation which includes myeloblasts and myelocytes. These mitotic cells then differentiate into the post-mitotic band cell that features indented and band-like nuclei. Band cells then fully differentiate into mature neutrophils with their characteristic segmented, multi-lobed nuclei. Throughout this process C-X-C motif chemokine receptor (CXCR) 1 is constitutively expressed, while CXCR2 becomes upregulated. Both are receptors for interleukin 8 (IL8), a chemokine associated with neutrophil activation. CXCR4, a receptor for stromal cell-derived factor-1, as well as integrin α4β1 (VLA4), which acts as a ligand for vascular cell adhesion protein 1 (VCAM-1), are downregulated during terminal differentiation. Both are involved in promoting retention of immature neutrophils in the bone marrow in order to prevent release of the cell into the circulatory system before differentiation into mature neutrophils is finished (3).

Once released from the bone marrow, circulating neutrophils remain in the bloodstream until they are recruited to a site of infection by a process referred to as extravasation. Endothelial cells at the site of infection express signaling ligands on their surface such as intercellular adhesion molecule 1 and 2 (ICAM-1, ICAM-2). These ligands are bound by neutrophil receptors selectin and integrin, which allow the

neutrophil to travel along the endothelium until they are signaled by chemokines from the endothelial cells to arrest movement and migrate between or through the endothelial cells to the site of infection. At the site of infection neutrophils use pattern-recognition receptors (PRRs) to detect pathogen-associated molecular patterns (PAMPs) expressed by microbes, as well as damage-associated molecular patterns (DAMPs) released by dying or dead host cells. Ligand binding to PRRs leads to intracellular signals that induce full activation of the neutrophil to combat invading pathogens (4).

Activated neutrophils are primed to employ various mechanisms to kill pathogens including release of cytotoxic granules (structures containing lysozymes, proteases and anti-microbial peptides that can break down the structure of the microbes) and reactive oxygen species (ROS), as well as phagocytosis, and the formation of neutrophil extracellular traps (NETs) - a process known as NETosis (4). The focus of this research concerns understanding the regulation of nuclear morphology dynamics during neutrophil activation prior to NETosis.

Neutrophils possess two different mechanisms for NETosis: NETosis leading to slow cell death and vital NETosis. These distinct forms of NETosis are triggered through exposure to different kinds of pathogens and activating stimuli. Vital NETosis involves NET formation via vesicles, small lipid bi-layer structures which transport proteins or other small molecules throughout the cytoplasm. In vital NETosis, these vesicles transfer bits of decondensed chromatin along with granule proteins to the cell membrane, where they are released outside of the cell as a NET. This method has been found to be much faster than cell death NETosis, taking between 5 minutes to an hour, and seems to leave the cell alive with its cell membrane intact and in some cases the cell is still capable of phagocytosis (5). The research of this thesis examines the effects of the proteins involved with the alternative NET mechanism, the slow cell death-mediated NETosis.

Slow cell death NETosis is associated with a change in nuclear morphology, where the lobed nuclear structure characteristic of neutrophil nuclei is lost as the nuclear envelope delobes to become circular. The nuclear membrane then disassembles, and the decondensed chromatin mixes with neutrophil granule proteins and is expelled from the cell to form an extracellular trap to contain and kill bacteria (5).

A variety of proteins and signaling pathways have been implicated in this mechanism of neutrophil activation and NETosis including nicotinamide adenine dinucleotide phosphate oxidase (NADPH-oxidase, NOX), neutrophil elastase (NE), myeloperoxidase (MPO), and peptidylarginine deiminase 4 (PAD4). Studies concerning slow cell death NETosis mainly utilize phorbol 12-myristate 13-acetate (PMA) as a chemical inducer along with calcium ionophores such as A23187, although each involves different pathways.

Various chemical and microbial stimulants can trigger slow cell death NETosis. PMA, one of the most common chemical stimulants used in neutrophil research, can activate several isoforms of protein kinase C (PKC) by passing through the cell membrane and acting like the secondary messenger molecule and PKC activator diacylglycerol (DAG). PMA cannot activate PKC isoforms that are not activated by DAG (6). PMA-induced NET formation relies upon the Raf-MEK-ERK pathway upstream of NOX activation and requires extracellular calcium stores for calcium influx (7, 8). PMA activation relies on the same pathways as activation induced by the microbes *Candida albicans* and Group B *Streptococcus* which lead to the activation of NOX (5). However, unlike PMA, activation induced by these microbes do not require calcium influx (9).

The PMA inducing activation pathway leading to NETosis involves the production of ROS by NADPH-oxidase 2, as well as MPO and NE, which are stored in azurophilic granules prior to neutrophil activation (5). Neutrophils require ROS and NOX2 to produce NETs, as the neutrophils from patients with chronic granulomatous disease (CGD), a disorder characterized by deficient NOX2-mediated superoxide production, are unable to perform NETosis in response to PMA (9, 10). Additionally, treatment with diphenyleneiodonium chloride (DPI) has been observed to reduce PMA-activated NET formation in human neutrophils (11). DPI is an all-NOX inhibitor that binds to the NOX enzyme near its NADPH binding site, preventing it from transferring an electron from the NADPH molecule to an oxygen molecule to form superoxide (12). ROS produced by NOX2 is also involved in the extracellular release of ROS and granules. The granule proteins, ROS, and hypochlorous acid (HOCl) contained within the exocytosed granules can destroy invading microbials. Phagocytic killing of microbes utilizes these same granules, as phagocytic

vesicles fuse with neutrophil granules (4). This makes NOX an important player in the neutrophil's overall anti-microbial activities, as it is required for both phagocytosis- and NET-mediated killing of microbes.

The granule protein MPO produces the HOCl found in granules by mediating a reaction between Cl^- ions and hydrogen peroxide, H_2O_2, a compound which can be formed from the superoxide made by NOX (4). In PMA-induced slow cell death NETosis, production of ROS by NOX2 leads to the release of MPO and NE from granules, allowing for their subsequent translocation to the nucleus (13, 14). Once in the nucleus, NE degrades the core histones H2B and H4 to cause the neutrophil chromatin to decondense (14). In vitro, MPO enhances chromatin decondensation in the presence of NE, independent of its enzymatic function. However, while NE addition to neutrophil nuclei alone is sufficient for chromatin decondensation, MPO addition is not sufficient. Work performed with the NE inhibitor GW311616A (NEi), which inactivates the site on the enzyme that cleaves peptide bonds, and the MPO inhibitor 4-aminobenzoic hydrazide (ABAH), which works by reducing MPO to its ferrous myeloperoxidase state to make it irreversibly inactive upon its reaction with hydrogen peroxide, further supports these findings (15, 16). NEi inhibits the decondensation of neutrophil nuclei while ABAH does not (14). However, ABAH treatment of human neutrophils decreases formation of NETs produced by PMA, a phenotype that is also seen with MPO-deficient human neutrophils (9). Due to the conflicting findings on MPO it is unclear as to how MPO's enzymatic activity is directly involved with PMA-induced chromatin decondensation and subsequent NET formation, though its enzymatic activity does seem to contribute to the release of NE from the granules by an unknown mechanism (13). NE is a much clearer requirement for PMA-induced activation, as NEi inhibition of NE activity inhibits the production of NETs in response to PMA (9, 14). Additionally, NE can also contribute to the neutrophil's anti-microbial activities by the degrading virulence factors of bacteria extracellularly. As NE is still associated with chromatin once it becomes decondensed and the cell lyses to release the NET, it can directly aid the NET's ability to combat bacterial infection by enzymatically acting on the microbes trapped by the expelled NET (17).

A23187, a potent stimulator of NET formation, is an ionophore that facilitates transport of calcium ions across the plasma membrane by both acting as a calcium carrier and forming channels in the membrane

(18). The mobilization of calcium from both the extracellular space and the endoplasm reticulum are also involved in NETosis in response to IL8, a stimulator that naturally occurs at sites of infection (8). Ionophores can induce NETosis by inducing calcium influx in the cell and triggering calcium-sensitive signaling pathways. A23187-induced NETosis triggers PAD4-mediated histone deamination and requires the PKC isoform PKCζ (19). Deamination, or citrullination, is the post-translational modification of arginine residues to citrulline, changing the structure of the affected protein. PAD4 is known to translocate to the nucleus after calcium influx and citrullinate core histones H3, H2A, and H4, promoting chromatin decondensation and the formation of NETs (20).

Inhibition of PAD4 activity results in decreased A23187-induced NET formation in cells of the promyelocytic HL-60 cell line that were differentiated into neutrophil-like cells by dimethyl sulfoxide (DMSO) treatment. A23187 mimics stimulation with bacteria like *Shigella flexneri*, which also promote PAD4 histone citrullination in DMSO differentiated HL-60s. PAD4 inhibition during *Shigella flexneri* encounter is sufficient to decrease NET formation with DMSO differentiated HL-60s (20). Additionally, work with PAD4 inhibitor GSK484, which binds to residues at the active site of the enzyme, showed that PAD4 inhibition diminishes H3 citrullination and NET formation in response to the ionophore ionomycin in mouse neutrophils (21, 22). As such, H3 citrullination is associated with, and often serves as a marker for NETosis. However, the extent of PAD4's involvement in NETosis seems to be dependent the type of stimulus the neutrophil is exposed to, since it is not required with PMA-induced NETosis. Different neutrophil activating stimuli activate different isoforms of PKC, and only the PKCζ isoform has been observed to promote PAD4 activation (19). Furthermore, MPO-deficient human neutrophils are still able to perform NETosis in response to A23187, and, in contrast to PMA-induced NETosis, ABAH inhibition of MPO does not prevent A21387-induced NETosis. NE inhibition also does not affect A23187-induced NET formation, and CGD patient neutrophils, despite lacking NOX2, are also able to perform A23187-induced NETosis (9).

Both PMA and A23187 invoke the cell death-mediated NETosis mechanism, but both activate and rely upon different intracellular signaling pathways to do so. While PMA activation involves calcium influx

in its signaling pathway, it does not promote PAD4 activity. In fact, PKCα, which is activated by PMA, represses PAD4 histone deamination. This may explain why neutrophil activation by PMA does not require histone citrullination and why PMA can repress A23187 ionophore stimulated histone citrullination while still inducing NETosis. In line with this, PKCζ is one of the PKC isoforms that is not activated by PMA (19).

Neutrophil activation in response to pathogen encounter also has differing signaling and protein requirements depending on the pathogen. In the case of the fungus *Candida*, inhibition of PKC (PKCα and PKCβ1 specific inhibitor) decreases NET formation. However, PAD4 knockout does not inhibit *Candida* stimulated NET formation in mice even though *Candida* stimulation does promote PAD4 H3 citrullination similar to A23187 (9, 23). This suggests that PAD4 activation may, in this case, be a side effect of cell lysis and the accompanying extracellular calcium flux. The presence of ROS is required for NETosis induction by *Candida*, but as *Candida* is capable of inducing ROS bursts on its own, NOX2 is not required (9). Ultimately it seems that the signaling pathway for this NET formation mechanism showcases flexible signaling and protein requirements depending on the stimulus the cell encounters.

The neutrophil's lobed nuclear structure is a defining characteristic of this cell type. The way that chromatin is organized in the nucleus is known to be associated with the transcriptional activity of genes. The compartmentalization of chromatin is an important aspect of chromatin organization. Individual chromosomes form chromosome territories, wherein the chromatin of individual chromosomes stay in closer 3D proximity to themselves than to other chromosomes, limiting interchromosomal interactions and promoting intrachromosomal interactions. Within and across these territories chromatin segregates into compartments of heterochromatin and euchromatin, which are associated with repressed and active transcription, respectively. Chromatin within each chromosome is further organized into topologically associated domains (TADs), which are regions of the genome that have frequent physical interactions with themselves and few interactions with other regions. Genes within TADs are kept compartmentalized and insulated from interactions outside of the domain with boundary elements enriched for cohesin, CCCTC-binding factor (CTCF), and transcribed genes (24). These domains can be conversed across species (25).

Smaller scale chromatin interactions occur within TADs in the form of loop structures facilitated by cohesin and CTCF binding, where enhancers are brought into close proximity to the promoters of genes whose transcriptional activity they regulate (24).

The ability to both limit and promote activation of gene transcription with TADs and enhancer-promoter loops is important for normal genome functioning. CTCF binding sites at TAD boundaries are common among non-coding cancer mutations, suggesting that interference with normal TAD boundaries can lead to pathological misregulation of transcription (24). Additionally, in the case of myogenesis, it has been found that TADs can become enriched for cell-type specific genes and the morphology of chromosome territories can change after differentiation (26). This showcases how TAD compartments and changes in chromatin morphology can be associated with cell-type specific functioning and genetic transcription.

It is unclear as to the exact purpose the unique nuclear structure of neutrophils serves. It has been theorized that the more compact and flexible shape of the lobed nucleus aids neutrophils in passing between and through cells to infection sites (27, 28). In support of this theory, work with hypolobulated mouse neutrophils lacking the LaminB1 receptor (LBR) show deficiencies in migrating through membrane pores (29). Neutrophil activation is also known to induce a wide range of gene expression alterations, with different stimuli inducing both shared and differing changes in gene expression (30).

The lobed neutrophil nucleus has also been seen to influence its higher order chromatin organization. Change in nuclear morphology is associated with both the differentiation of granulocyte precursors into neutrophils and the activation of neutrophils. Differentiation causes the circular nuclei of progenitor cells to form distinct lobes. Alternatively, activation causes nuclear delobing, returning the nucleus to a circular structure (3, 10). Changes in neutrophil nuclear morphology have been studied previously in the Murre lab. Work with the mouse neutrophil progenitor cell-line ECOMG have shown that once differentiated, pericentromeric and centromeric heterochromatin are recruited to the lamina, and that knockout of LBR prevents both this repositioning of the heterochromatin and the usual nuclear morphological changes associated with neutrophil differentiation. This suggests that the repositioning of pericentromeric and centromeric heterochromatin is involved with forming the neutrophil's characteristic

lobed nuclear shape. It was also seen using ECOMGs that differentiation induced changes in chromatin interactions and compartmentalization. In this system, differentiation is accompanied by an enrichment of interactions among and between heterochromatic loci genome-wide (31).

Recent work in the Murre lab has investigated how human neutrophil genomic interactions compare to other cell-types and how these interactions change in response to activation. In neutrophil nuclei chromosome territories are maintained and distributed throughout individual lobes. Genome-wide chromosome conformation capture (Hi-C) (32) has shown that interactions between smaller chromosomes are proportionally increased in human neutrophils, while interactions between larger chromosomes and between small and large chromosomes are proportionally decreased compared to human embryonic stem cells (hESCs) as well as differentiated human cell types (Denholtz M, personal communication). When stimulated with PMA, human neutrophils become delobed, and interactions between larger chromosomes and between small and large chromosomes become proportionally increased compared to unstimulated neutrophils, making it more similar to the interactions seen in the rounded nuclei of non-neutrophils (Denholtz M, personal communication). Based on how stimulation results in changes in gene expression and chromosome interactions, it is clear that this morphological change is associated with neutrophils' ability to become activated and perform NETosis. Therefore, changes in the normal functioning of the neutrophil stimulation pathways may affect the nuclei's ability to change its shape and enter an activated state. A genetically tractable model with which to analyze changes in nuclear morphology throughout neutrophil differentiation and stimulation would greatly aid research concerning neutrophil activation, nuclear morphology, chromatin organization, and gene regulation.

The purpose of this research is to establish the promyelocytic HL-60 cell line as a genetically tractable model for studies of neutrophil nuclear morphology dynamics prior to NET formation, and to use this model to further our understanding on what elements of the neutrophil activation pathway contribute to these dynamics. HL-60s are able to differentiate into neutrophil-like cells through treatment with DMSO, all-trans retinoic acid (ATRA), and dimethylformamide (DMF), making them a useful model cell with which to visualize differences in neutrophil nuclear shape.

HL-60 differentiation by different chemicals act by different pathways. Little is known concerning the mechanisms behind DMF-induced differentiation of HL-60s, but ATRA and DMSO treatment both result in the downregulation of c-myc, a proto-oncogene that encodes a transcription factor which activates cell growth related genes, and upregulation of calcium-binding proteins MRP8 and MRP14 (33). HL-60 differentiation with different retinoids, including ATRA, results in upregulation of differentiation genes, molecules which aid in neutrophil adhesion to the endothelium, and the NOX activation pathway. Even with retinoids of similar types however, there remain differences in gene regulation during differentiation. This includes the upregulation of ubiquitin pathway genes and signal transduction genes by ATRA-induced differentiation but not when differentiation was induced by the retinoid N-(4-hydroxycarbophnyl)-retinamide (RII) (34). Likely due to different differentiation pathways, ATRA dHL-60s only form NETs in response to PMA and DMF dHL-60s form NETs in response to both PMA and A23187. Additionally, ATRA most efficiently differentiates cells into neutrophil-like cells in terms of change in nuclear morphology but seemed to be deficient in producing the usual calcium flux and citrullination of histone H3 associated with stimulation (35). Ultimately, differentiation by different chemicals produces cells with differing reactions to stimuli, and therefore seems to differentiate HL-60s through different mechanisms.

Herein we use a panel of chemicals known to inhibit various biological processes associated with NET formation, namely the activity of proteins NOX, MPO, NE, and PAD4, to determine the role of these processes in modulation of neutrophil nuclear morphology. Using immunofluorescence staining for the nuclear envelope protein LaminB1, we calculated the circularity of hundreds of HL-60 nuclei differentiated with either ATRA or DMF and activated with PMA or A23187. By quantifying changes in nuclear circularity during activation and inhibition of these changes with chemical inhibitors, we have identified which proteins are required for dHL-60 nuclear shape changes prior to NETosis.

MATERIALS AND METHODS

HL-60 Culture and Differentiation

Cells were cultured in IMDM (Life Technologies, 12440-053) with 20% Fetal Bovine Serum (Atlanta, S11550) and 1X Penicillin-Streptomycin-Glutamine (Life Technologies, 10378016) and incubated at 37°C and 5% CO_2, with the media replaced every 3 days. Cell were differentiated with 5-day incubation period in culture media with either 1µM ATRA (Sigma-Aldrich, R2625-100MG) in EtOH (Decon Labs, V1016), 70mM DMF (Sigma-Aldrich, 227056-100ML), or 1.3% DMSO (Sigma-Aldrich, D1435-500ML), and incubated at 37°C and 5% CO_2. The ATRA media was replaced every day while the DMF media was replaced on either the 2nd or 3rd day of differentiation. A 1mM working stock of ATRA in EtOH kept at -20°C was used with the ATRA media freshly prepared every day, with the stock being replaced with new ATRA every two weeks.

Blood Draws and Neutrophil Isolations

Neutrophils were harvested from whole human blood in accordance with approved protocols for anonymized human subjects at the University of California, San Diego. Venous blood was drawn into heparinized syringes. Whole blood was layered onto Polymorphprep reagent (Accurate Chemical and Scientific Corp., AN1114683) and was centrifuged for 45 minutes at 500g, 25°C, and allowed to stop without breaking. Granulocyte layer was extracted and contaminating red blood cells were lysed as needed (generally 1-3 times) with brief resuspension in H_2O followed by flooding with 1x phosphate buffered saline (PBS) and centrifugation at 500g for 7 minutes at 25°C. Cells were checked for purity via wright-giemsa staining; the final granulocyte fraction was generally >95% neutrophils. Except where otherwise stated, neutrophils were cultured in HBSS (Thermo Fisher, 14025092) with the addition of 0.5% endotoxin-free BSA (Akron, AK8917-0100) at 37°C in a humidified incubator.

Wright-Giemsa Staining

Cells were spun in Eppendorf tubes at 400G and resuspended in 1x Dulbecco's Phosphate Buffered Saline (DPBS) (Life Technologies, 14190-144), then spun onto coverslips with a cyto-spinner for 3 minutes at 1000rpm. Cells were stained with wright stain (Sigma-Aldrich, WS16-500ML) for 3 minutes. The wright stain was removed, and the cells were washed with MQ water 6 times. Once dried, cells were stained with 1:10 giemsa stain (Sigma-Aldrich, GS500-500ML) for 7 minutes. The stain liquid was removed, and the cells were washed with MQ water 6 times. Coverslips were mounted with mounting media.

Stimulation and Inhibitor Treatment

Cells were resuspended in 1ml of new media with 100nM PMA (Promega, V1171) in DMSO or 50μM A32187 (Sigma-Aldrich, C7522-5MG) in DMSO and incubated for 3 hours or 1 hour respectively at 37°C and 5% CO_2. Unstimulated cells were incubated for same amount of time with an equivalent amount of DMSO. Stimulations were performed with between 1x10^5 to 3x10^5 cells per condition. For experiments involving inhibitor treatment, cells were resuspending in 0.5ml new media with inhibitor for 1-hour pre-treatment (DPI (Sigma-Aldrich, 43088-5G) 100μM in DMSO, GW311616A (Axon Medchem, GW 311616A) 20μM in water, ABAH (Sigma-Aldrich, A41909-10G) 500μM in DMSO, and GSK484 (Cayman Chemical, 17488) 50μM in DMSO). After pre-treatment 0.5ml of media containing both inhibitor and either the PMA or A23187 stimulus was added for cell stimulation. Untreated cells were incubated for the same amount of time with an equivalent amount of DMSO with exception of GW311616A experiments. Cells were collected and spun down in an Eppendorf tube at 300G, washed once with 1x DPBS, and fixed with 4% PFA (Electron Microscopy Science, 15710) in 1x DPBS for 10 minutes. Cells were then washed 3 times with 1x DPBS and resuspended in 1x DPBS, then spun onto coverslip with a cyto-spinner centrifuged for 3 minutes at 1000rpm. Cells were stored in 1x DPBS at 4°C until Immunofluorescent (IF) staining.

Immunofluorescent Staining

Cells on coverslips were first washed with 0.5% Triton (Sigma-Aldrich, RES9690T-A101X) in 1x PBS for 5 minutes, and then washed with 0.05% Tween (Sigma-Aldrich, P9416-100ML) in 1x PBS for 5 minutes 3 times. Cells were then incubated at room temperature with Donkey Block (1x PBS, 3% Donkey Serum (Sigma-Aldrich, D9663-10ML), 0.05% Tween, 1x BSA (VWR, 2930)) for 30 minutes. IF staining was performed with 1:200 Rabbit α-LaminB1 (Proteintech, 12987-1-AP) in 1x PBS at 4°C overnight. 3 5-minute washes with 0.05% Tween in 1x PBS were performed before 1-hour incubation in the dark with 1:500 Donkey α-Rabbit 488 (Thermofisher Scientific, A21206) in Donkey Block at room temperature, which was subsequently followed by 3 more 5-minute washes with 0.05% Tween and 1x PBS, with the 2nd wash containing 1:5000 4′,6-diamidino-2-phenylindole (DAPI) (Sigma-Aldrich, 10236276001). Coverslips were mounted with ProLong™ Gold Anti-fade Reagent (Life Technologies, P36934).

IF Imaging and Analysis

Images were taken of the cells in the green and blue channel with the Zeiss Airyscan 880 microscope at 20x and raw images were processed with Airyscan Processing. ImageJ software (36) was used to threshold the LanminB1 fluorescence, to produce outlines of the nuclei, and to measure the nuclear envelope circularity. 3x3 tiled images were stitched together with the Grid/Collection Stitching plugin (37) for ImageJ before analysis. Threshold settings were set at default, red, and dark background. The Analyze Particles function in ImageJ was used to measure all metrics. For single tiled images, measured particle size was limited to 15 microns^2 and above. For 3x3 tiled images, measured particle size was limited to 6000 microns^2 and above. Measurements were then loaded into RStudio (38) and boxplots of the circularity measurements were generated. To exclude measurements of clumped cells identified as very large single cells by ImageJ, area cut-offs in square pixels based on each cell-types' spread of area measurements were implemented. Only measurements of particles (nuclei) equal to or below the cut-off were used in the

boxplots. For single tiled images, the area cut-offs were 90 for undifferentiated HL-60s, 60 for ATRA dHL-60s, and 70 for DMF dHL-60s. For 3x3 tiled images, the area cut-off was set to 25000 for all samples.

RESULTS

In order to establish the promyelocytic HL-60 cell line as a genetically tractable system with which to study neutrophil nuclear morphology, we needed establish robust differentiation protocols as well as strong quantitative methods with which to study nuclear structure in these cells. Initially, giemsa staining was used to visualize the change in HL-60 nuclear morphology brought on by a 6-day time course in culture (Figure 1a) or 6-day differentiation treatments with either DMSO, ATRA, or DMF (Figures 1b-d, respectively). We found that HL-60 nuclei cease to increase lobularity after 5 days of differentiation (data not show). At this time point differentiated HL-60 (dHL-60) nuclei had acquired a fully lobulated structure reminiscent of a primary human neutrophil (Figure 1e), or a band-like nuclear morphology phenotype (Figure 1b, top-right cell, for instance). Differentiation by DMSO was associated with more cell death throughout the differentiation time course than either ATRA or DMF differentiation (Figure 2), as such,

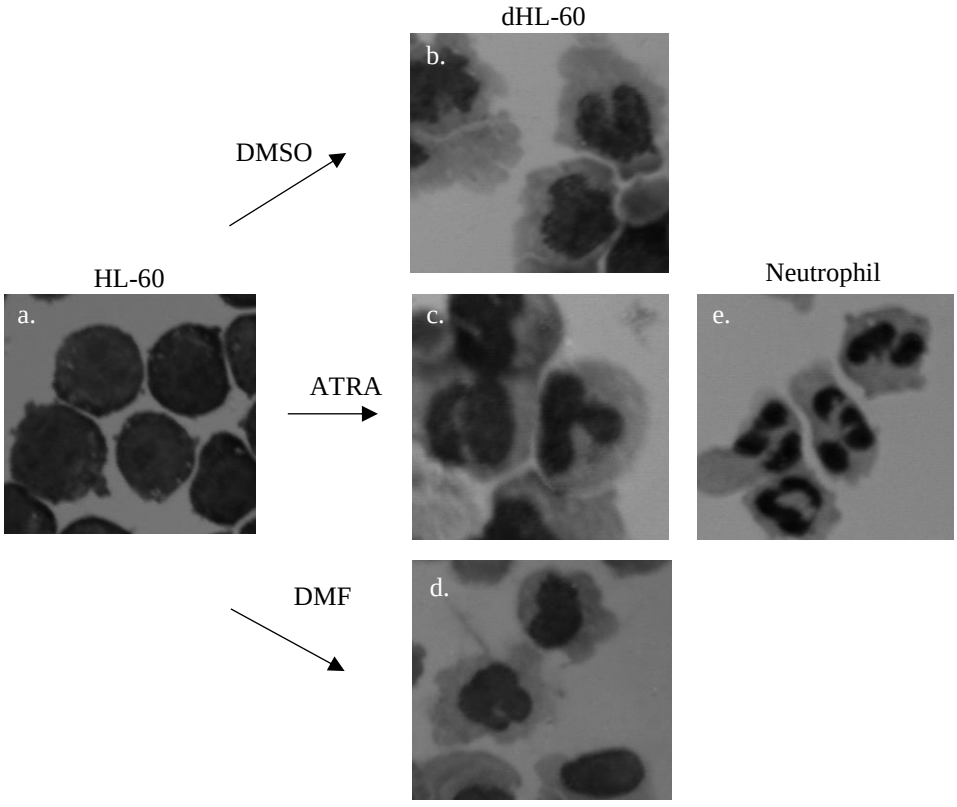

Figure 1. HL-60s differentiate into neutrophil-like cells with similar nuclear morphology. Giemsa stain of a) undifferentiated HL-60s, day 5 b) DMSO dHL-60s, c) ATRA dHL-60s, d) DMF dHL-60s, and e) primary human neutrophils.

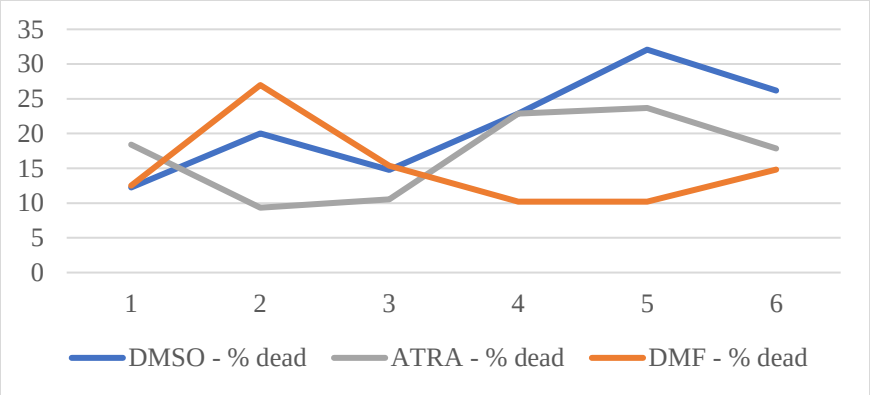

Figure 2. Cell death during treatment of HL-60s with various chemical inducers of HL-60 differentiation. Percentage of dead cells each day throughout the 6-day DMSO, ATRA, or DMF-induced differentiation of HL-60s based on trypan blue exclusion cell counts.

subsequent experiments used ATRA and DMF differentiation for 5 days to generate ATRA dHL-60s and DMF dHL-60s, respectively.

In order to study nuclear morphology quantitatively, analysis of nuclear circularity was assessed as a metric for quantifying differentiation-induced changes in nuclear morphology. Undifferentiated HL-60s and 5-day ATRA or DMF dHL-60s were fixed and immunofluorescent staining for LaminB1 was used to visualize their nuclear envelopes, and DAPI was used to visualize their DNA (Figure 3a). Outlines of the nuclear envelope based on the LaminB1 staining were produced by ImageJ (36) and served as representative objects to quantify (Figure 3b). Circularity of these outlines was then measured in ImageJ for every nucleus across each condition on a scale of 0 to 1, with 1 being a perfect circle. The distributions of these circularity measurements were then compared between conditions (Figure 3c).

To confirm the utility of the circularity quantification, and to assure that it was an accurate representation of experimentally observed qualitative nuclear morphologies, we first compared the circularity of the dHL60's to their undifferentiated counterparts. ATRA dHL-60s had significantly lower nuclear circularity compared to undifferentiated HL-60s (i.e.: they are less circular and more lobed). However, DMF dHL-60s nuclei were found to be significantly more circular compared to undifferentiated HL-60s. Based on the LaminB1 stain, DMF dHL-60s can be visually distinguished from undifferentiated HL-60s due to the presence of folded creases on their nuclear envelope that are not typically seen on undifferentiated cells (Figure 3a shows an example of this). This creasing cannot be captured by the ImageJ

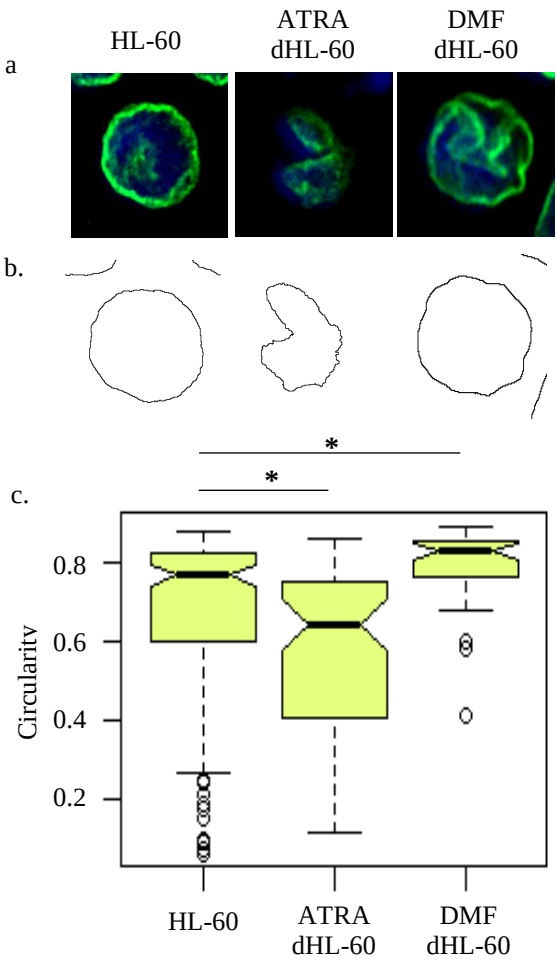

Figure 3. HL-60 differentiation results in changes in nuclear morphology. a) LaminB1 IF staining of undifferentiated HL60s, ATRA dHL-60s, and DMF dHL-60s. LaminB1 stain is green and DAPI is blue. b) Corresponding ImageJ produced LaminB1 outlines of stained nuclei. c) Boxplots of nuclear circularity data (HL-60 n =197, ATRA dHL-60 n = 69, DMF dHL60 n = 42). * = Wilcoxon rank sum test p-value < 0.05.

outline (Figure 3b), and therefore does not impact the cells' circularity measurements. This makes the DMF dHL-60s' average nuclei circularity comparable to undifferentiated HL-60s. ATRA differentiation can induce nuclear shape change that is closer to the standard neutrophil multi-lobed morphology, making their changes dramatic enough to be indicated in the outline and circularity measurements (Figure 3b-c).

The same procedure was then used to assess the usefulness of nuclear circularity as a metric for quantifying activation induced changes in dHL-60 nuclear morphology. It was found that PMA stimulation

of ATRA dHL-60s caused a significant increase in their nuclear circularity, while A23187 ionophore stimulation of ATRA dHL-60s did not (Figure 4a-c). While A23187 stimulation of DMF dHL-60s did cause a general increase in nuclei circularity, both visually and quantitatively, this difference in the initial experiment was not statistically significant (Figure 5a-c). However, data pooled from across three separate experiments shows that the modest A23187-induced increase in nuclear circularity seen in individual experiments gains statistical significance in aggregate (Figure 5d). No change in circularity was induced by PMA stimulation for DMF dHL-60s, either visually or quantitatively (Figure 5a-c). These findings indicate that circularity can be used to measure changes in nuclear morphology of ATRA dHL-60s brought on by PMA stimulation, as well as changes to DMF dHL-60 nuclei brought on by A23187 stimulation.

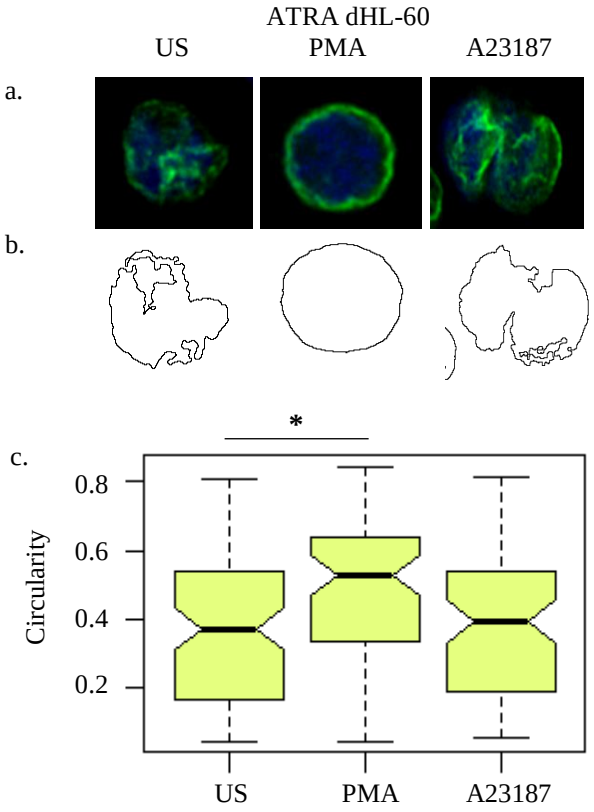

Figure 4. ATRA dHL-60 stimulation with PMA results in increased nuclear circularity. a) LaminB1 IF staining of ATRA dHL-60s. LaminB1 is green and DAPI is blue. b) Corresponding ImageJ-produced LaminB1 outlines of stained nuclei. c) Boxplots of nuclear circularity (Unstimulated n = 91, PMA n = 64, A23187 n = 71). US = unstimulated, * = Wilcoxon rank sum test p-value < 0.05.

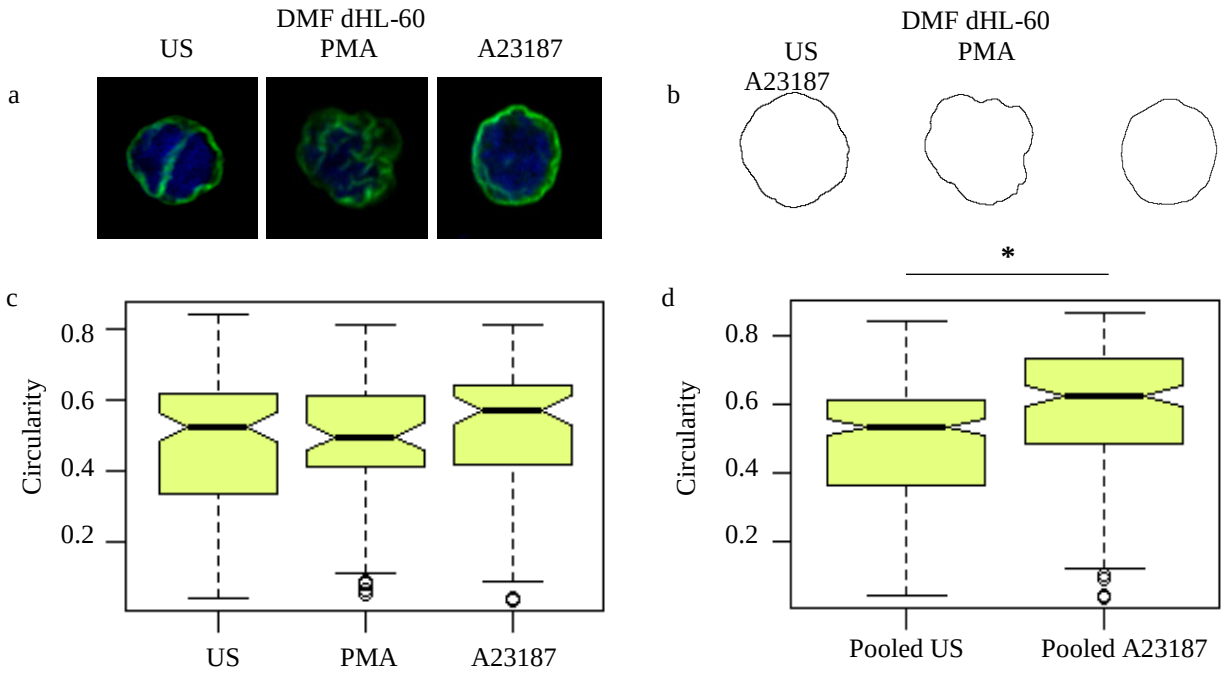

Figure 5. DMF dHL-60 stimulation with A23187 results in increased nuclear circularity. a) LaminB1 IF staining of DMF dHL-60s. LaminB1 is green and DAPI is blue. b) Corresponding ImageJ-produced LaminB1 outlines of stained nuclei. c) Boxplots of nuclear circularity (Unstimulated n = 120, PMA n = 78, A23187 n = 82). d) Boxplots of unstimulated and A23187 stimulated DMF dHL-60 nuclear circularity pooled from 3 separate experiments (Unstimulated n =282, A23187 n = 165). US = unstimulated, * = Wilcoxon rank sum test p-value < 0.05.

As discussed in the introduction, a variety of proteins and biological processes are known to contribute to NETosis in various activating contexts. To ascertain whether these processes and proteins are required for the observed changes in nuclear morphology during dHL-60 activation, chemical inhibitors of known neutrophil activation pathways and proteins were used, and their effects on stimulation-induced changes in dHL-60 nuclear morphology were quantified.

To observe the affect NOX has on dHL-60 activation-induced nuclear morphology changes, ATRA dHL-60s were pretreated with DPI, a NOX inhibitor, before and throughout PMA stimulation. As was found previously, ATRA dHL-60 nuclei undergo substantial delobulation upon PMA stimulation (Figures 6a-b). The PMA stimulated DPI treated ATRA dHL-60s nuclei, however, failed to increase nuclear circularity compared to DMSO control PMA stimulated ATRA dHL-60s, although this difference was not statistically significant (Figure 6b). Qualitative review of the LaminB1 staining shows that this low

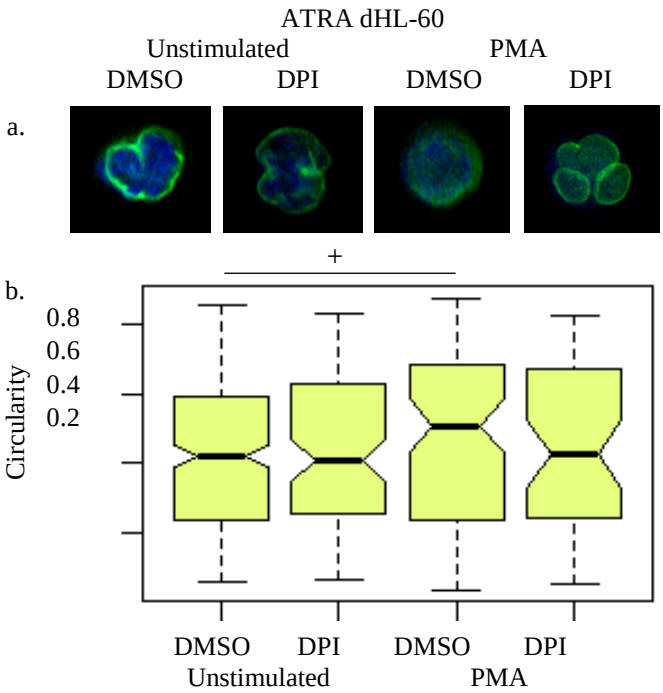

Figure 6. Inhibition of NOX prevents PMA-induced change in nuclear circularity in ATRA dHL-60s. a) LaminB1 IF staining of ATRA dHL-60s. LaminB1 is green and DAPI is blue. b) Corresponding boxplots of nuclear circularity (Unstimulated: DMSO n = 304, DPI n = 91. PMA: DMSO n = 85, DPI n = 50). + = Wilcoxon rank sum test p-value of 0.092.

circularity reflects a true inhibition of PMA-induced increase of in nuclei circularity, suggesting that inhibition of NOX blocks the PMA induced increase in nuclear circularity.

To determine the role of MPO in activation-induced nuclear morphology changes, ATRA dHL-60s were treated with ABAH before and throughout PMA stimulation. The PMA stimulation significantly increased the circularity of the ATRA dHL-60 nuclei, and ABAH treatment was not able to inhibit this increase, though the median value of the circularity data is non-significantly lower than DMSO control (Figure 7a-b). Based on qualitative review, the majority of the PMA stimulated ABAH treated cells became highly circular, similar to the PMA DMSO condition. Most likely, the inhibition of MPO by ABAH does not inhibit the delobulation of dHL-60 nuclei during PMA activation.

To explore the role of NE on dHL-60 activation-induced changes in nuclear morphology, ATRA dHL-60s were pretreated with NEi before and during PMA stimulation. Again, PMA treatment induced an increase in nuclei circularity of the ATRA dHL-60s (Figure 8a-b). The cells treated with NEi remained

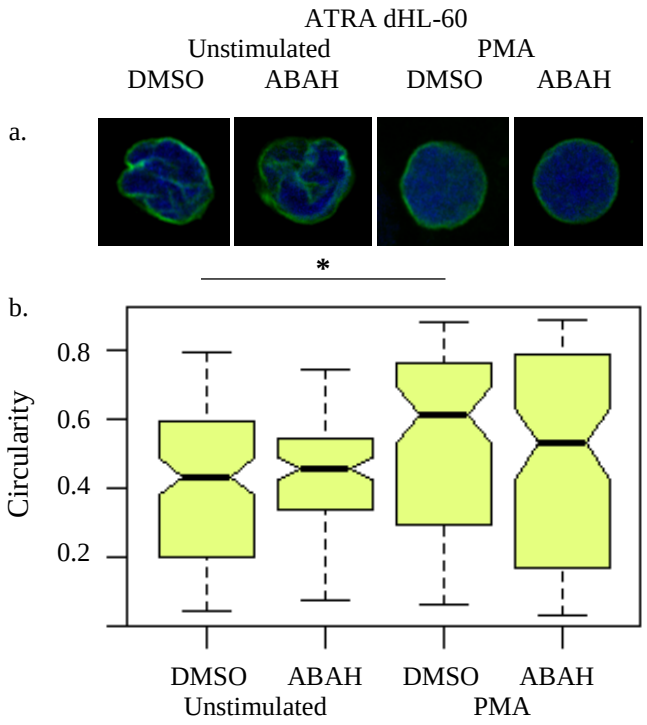

Figure 7. Inhibition of MPO does not prevent PMA-induced changes in ATRA dHL-60 nuclear circularity. a) LaminB1 IF staining of ATRA dHL-60s. LaminB1 is green and DAPI is blue. b) Corresponding boxplots of nuclear circularity (Unstimulated: DMSO n = 123, ABAH n = 125. PMA: DMSO n = 83, ABAH n = 88). * = Wilcoxon rank sum test p-value < 0.05.

lobed, showing a lower nuclear circularity than PMA stimulated ATRA dHL-60 cells (Figure 8b). The cell count was fairly low for those two conditions, so this difference in circularity between the two samples was not statistically significant. Qualitative review of the LaminB1 staining showed that nuclei of PMA stimulated NEi treated dHL-60s remained lobular and comparable to the nuclei of unstimulated ATRA dHL-60s. This inhibition of delobulation is likely an accurate reflection of the NEi treatment preventing PMA-induced nuclei morphology changes.

To determine the role of PAD4 on dHL-60 activation-induced nuclear morphology changes, ATRA dHL-60s and DMF dHL-60s were treated with GSK484 before and during PMA or A23187 stimulation. A23187 stimulation caused a significant increase in DMF dHL-60s nuclei circularity (Figure 9a). GSK484 treatment significantly inhibited the gain in nuclear circularity induced by A23187 in DMF dHL-60s compared to A23187-activated DMSO control cells (Figure 9a-b). GSK484 treatment also affected

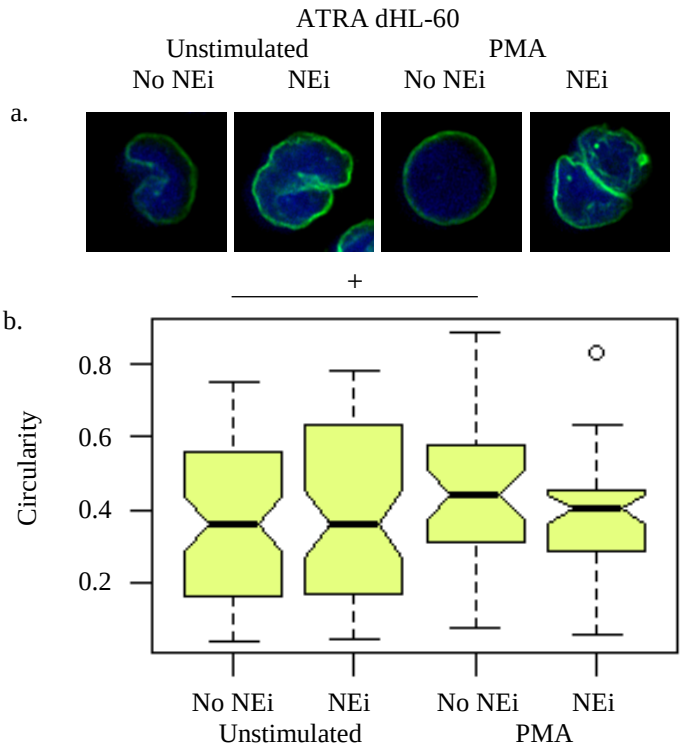

Figure 8. Inhibition of NE prevents PMA-induced change in circularity in ATRA dHL-60 nuclei. a) LaminB1 IF staining of ATRA dHL-60s. LaminB1 is green and DAPI is blue. c) Corresponding boxplots of nuclear circularity (Unstimulated: No NEi n = 73, NEi n = 59. PMA: No NEi n = 38, NEi n = 47). + = Wilcoxon rank sum test p-value of 0.075

unstimulated DMF dHL-60 nuclear morphology, but caused an increase in nuclear circularity rather than a decrease. This increase was found be significantly lower than the A23187-induced increase in nuclear circularity. Together these results demonstrate that PAD4 inhibition can block the A23187-induced increase in nuclear circularity in DMF dHL-60s.

GSK484 treatment also affected ATRA dHL-60s, in that it caused an increase in nuclear circularity in PMA stimulated GSK484 treated cells compared to PMA stimulated DMSO control cells. Additionally, it decreased nuclear circularity in GSK484 treated unstimulated cells compared to unstimulated DMSO control cells (Figure 9d). There is no definitive answer as to why this would occur, but the inhibitor may be introducing some variability to the samples. Even with these factors, the GSK484 failed to block stimulation induced increase in nuclear circularity, so it seems likely that PAD4 inhibition does not inhibit PMA-induced changes in nuclear morphology of ATRA dHL-60s (Figure 9c-d).

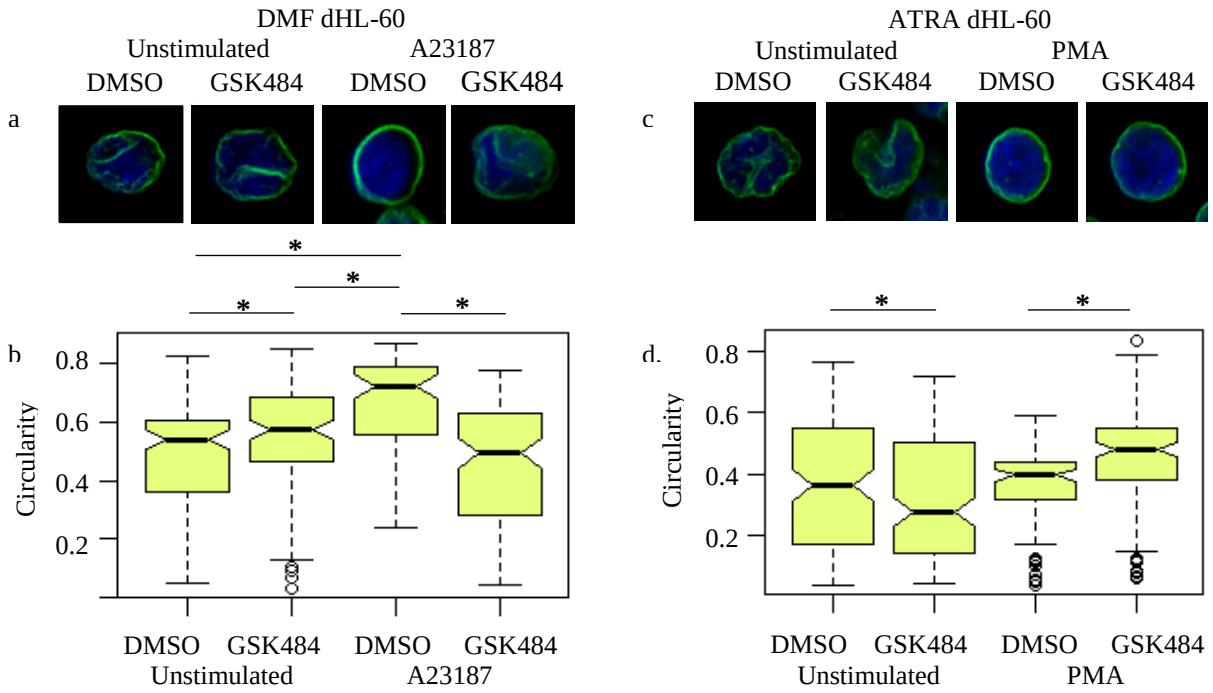

Figure 9. Inhibition of PAD4 enzymatic activity prevents A23187-induced change in circularity in DMF dHL-60 nuclei, but not PMA-induced changes in ATRA dHL-60 nuclei. a) LaminB1 IF staining of DMF dHL-60s. LaminB1 is green and DAPI is blue. b) Corresponding boxplots of nuclear circularity (Unstimulated: DMSO n = 136, GSK484 n = 126. A23187: DMSO n = 69, GSK484 n = 103). c) LaminB1 IF staining of ATRA dHL-60s. LaminB1 is green and DAPI is blue. d) Corresponding boxplots of nuclear circularity (Unstimulated: DMSO n = 134, GSK484 n = 162. PMA: DMSO n = 99, GSK484 n = 130). * = Wilcoxon rank sum test p-value < 0.05

DISCUSSION

The findings of this thesis demonstrate that HL-60s are a practical model cell for studies of differentiation- and activation-induced neutrophil nuclear morphology dynamics, and identify various pathways required for NETosis that are also required for pre-NETosis changes in nuclear shape.

Changes in the ImageJ-measured nuclear circularity successfully reflected the increase in lobularity in the dHL-60 nuclear morphology induced by ATRA differentiation, but not DMF differentiation (Figure 3.c). As ATRA differentiation is known to produce a more dramatic increase in lobularity of the dHL-60 nuclei, while DMF differentiation causes a subtler change by inducing creasing in the nuclear envelope that cannot be indicated by the ImageJ produced LaminB1 outline, it is expected that only ATRA-induced differentiation would produce a decrease in nuclear circularity. Contrary to expectations, DMF differentiation led to a significant increase in the circularity of the nuclei. Qualitative review of the undifferentiated HL-60 nuclei shows that they can range from being perfectly circular to lopsided or more elliptical in shape, while the outlines of DMF dHL-60 nuclei skews towards being more perfectly circular. There is no definitive answer for why the DMF dHL-60 nuclei are more circular, but it might be related to the DMF dHL-60 nuclei being more compact than undifferentiated HL-60 nuclei, making them less affected by extracellular forces that could push on the cell in a way to physically affect the shape of the nuclei, such as being next to other cells. It could also be that the undifferentiated HL-60 nuclei are naturally more heterogeneous in terms of the overall shape of the nuclei, and differentiation reduces this heterogeneity.

Nuclear circularity was also able to reflect stimulation-induced nuclear morphology dynamics. Specifically, changes in ATRA dHL-60 nuclear morphology upon activation rely upon similar pathways to the PMA-induced NETosis activation pathway of primary neutrophils. Similarly, DMF dHL-60 nuclear dynamics recapitulate the A23187-induced NETosis activation pathway (Figure 10). Together, these two different differentiation pathways cover two of the most common NETosis stimuli utilized in neutrophil studies, and allow for mechanistic dissection of the pathways required for the nuclear shape changes preceding NETosis.

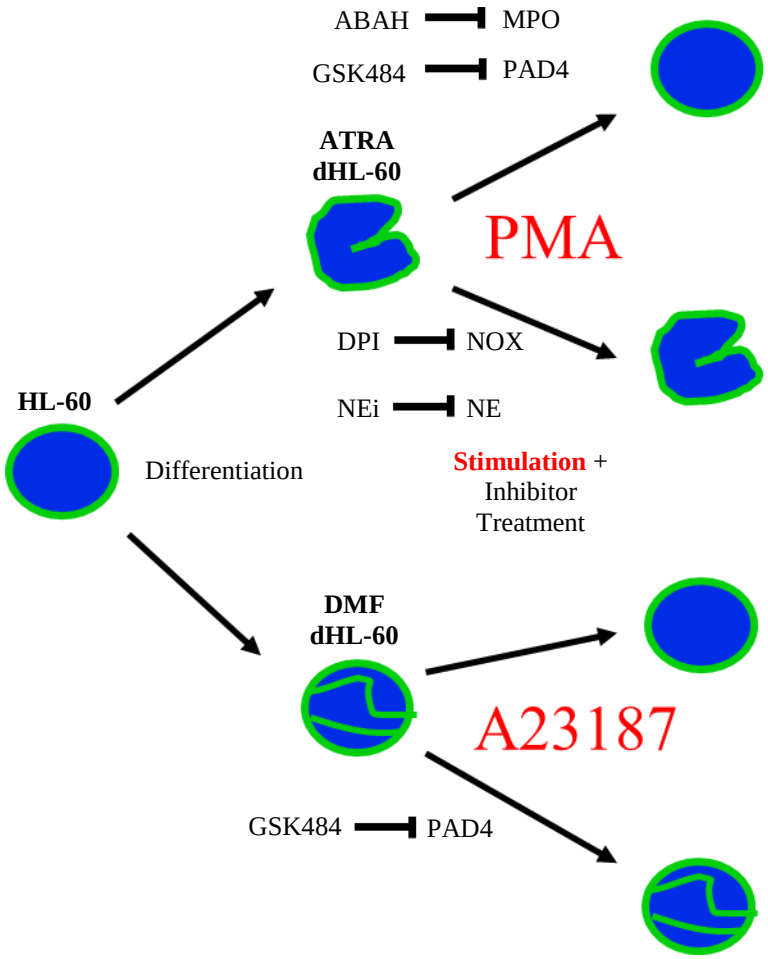

Figure 10. Schematic of HL-60 differentiation, stimulation, and inhibitor treatment results. Showcases how HL-60s can be differentiated into cells with neutrophil-like nuclear morphology using either ATRA or DMF, and how stimulation with PMA and A23187 respectively will cause nuclear shape to revert to being round. These activation-associated nuclear morphology dynamics can be prevented by inhibiting various proteins important for activation pathways.

Quantification of changes in nuclear circularity was able to reflect the loss of neutrophil lobularity and return to standard round nuclear shape upon stimulation of PMA of ATRA dHL-60s and A23187 ionophore of DMF dHL-60s (Figure 10). Conversely, A23187 stimulation of ATRA dHL-60s and PMA stimulation of DMF dHL-60s did not result in changes in nuclear morphology (Figure 4c and Figure 5c). As ATRA dHL-60s do not undergo normal functioning concerning the calcium influx pathway that A23187 is entirely dependent on (35), the lack of delobulation and associated increase in circularity most likely reflects how the ATRA dHL-60s failed to become successfully activated by the A23187, and thus failed to change the shape of the nuclei. This finding is confirmed by qualitative review of the LaminB1 images.

ATRA PMA stimulation and DMF A23187 stimulation both become activated and produce NETs in response to those respective stimuli, and this data confirms these stimulants also induce changes in nuclear morphology, and therefore changes in circularity. On the other hand, it is also expected for DMF dHL-60s to react to PMA stimulation as they have been seen to be capable of being activated by PMA and performing PMA-induced NETosis (35). However, while the phenotype of complete delobing of neutrophil nuclei is associated with the cells performing NETosis, there is no guarantee that change in nuclear shape is a requirement to produce a NET, as only a portion of the activated neutrophils that undergo nuclear morphological changes actually make NETs when encountering a NETosis stimulant, and there is no guarantee that all NETosis-inducing stimuli change the neutrophils' nuclear morphology in the exact same manner. It could be that the DMF dHL-60s are reacting to the PMA stimulation, but not in a way that is associated with dramatic change in nuclear morphology. One follow-up that could be performed to check this would be to measure the production of ROS by the PMA stimulated DMF dHL-60s. With PMA stimulation, production of ROS is often used as an alternative method to discern whether neutrophils are activated, along with their ability to perform NETosis, due to how heavily linked NOX activity and ROS production is with that pathway.

Inhibition of different known neutrophil NETosis pathway proteins were seen to also inhibit changes in nuclear morphology induced by stimulation depending on the stimulus the differentiated cells were reacting to. Based on the dHL-60s as a model and ImageJ-defined nuclear circularity as an indicator for nuclear morphology dynamics, inhibitor treatments implicated NOX and NE activity as being necessary for PMA-induced activation-associated delobing of neutrophil nuclei, while MPO and PAD4 are not. Along with this, PAD4 was shown to be necessary for A23187-induced activation associated delobing of neutrophil nuclei (Figure 10).

It was found that inhibition of NOX and NE blocked the increase of nuclear circularity induced by PMA stimulation of ATRA dHL-60s, while inhibition of MPO and PAD4 did not (Figure 6b, Figure 7b, Figure 8b, and Figure 9d). It is already known that inhibition of NOX or NE inhibits PMA-induced NET formation by primary human neutrophils, though in the theorized mechanism of NETosis, NE's main

contribution of chromatin decondensation is in the later stage of pre-NETosis activation which occurs after delobing (9, 11, 14). These results add to the neutrophil activation narrative that NOX and NE activity are also required for PMA-induced changes in nuclear morphology for ATRA dHL-60s. Additionally, inhibition of PAD4 fails to block both PMA-induced NETosis (14) and PMA-induced changes in nuclear morphology. Though the PMA stimulation of the PAD4 inhibitor experiment did not feature as dramatic an increase in nuclei circularity as expected from other experiments, and the inhibitor alone seemed to affect the circularity of the unstimulated dHL-60s, so repeat of this experiment may be beneficial to ensure the accuracy of these findings.

Despite MPO being a known regulator of PMA-induced NETosis in human neutrophils, ABAH inhibitor treatment failed to prevent PMA-induced increase in nuclear circularity. The role MPO plays in the activation of NETosis is known to be somewhat different than that of the absolutely required NOX and NE, since ABAH treatment of primary human neutrophils and partial MPO-deficiency only produces in a delay and decrease in NET formation rather than complete inhibition, and only complete MPO-deficiency produces complete inhibition of PMA-induced NETosis (39). Considering this, while MPO does play some role in NETosis, it is likely that MPO enzymatic activity is simply not involved with PMA-induced nuclear morphological changes. It was also found that PAD4 inhibition blocks A23187-induced nuclear morphological change with DMF dHL-60s, which complements the knowledge that PAD4 inhibition also inhibits ionophore-induced NETosis by primary human neutrophils as well as A23187-induced NETosis by DMSO dHL-60s (20, 21).

The biggest concern with this data is the occasional lack of statistical significance in the inhibitor treatments' effect on nuclei circularity as well as the occasional variation in the magnitude of the stimulation's effect on nuclei circularity. The overall spread of the nuclear circularity data tended to be fairly wide across most experiments, which likely made it difficult to produce statistically significant results. While qualitative review of the LaminB1 staining was used to determine if the differences in nuclei circularity indicated by the boxplots truly reflected the visual change in dHL-60 nuclear morphology, ideally circularity as a quantitative metric for observations of these dynamics should be able to signify

meaningful trends on its own. As aggregating the circularity measurement data from across multiple experiments was seen to help improve the statistical significance of the data's trend (Figure 5d), I suggest repeating experiments or increasing the number of cells imaged for analysis in order to ensure the quality of the data. Additionally, this method showcased that changes in imaging parameters, such as using tiled images, changing the number of tiles contributing to tiled images, and changing the overlap of the tiles can lead to differing analytical results that are inconsistent with the LaminB1 staining's qualitative indication of the cells' nuclear morphology. Changes in the software measurement parameters such as changing the size limits on the particles that can be measured can also lead to differing results. I advise that future uses of this method be done with ensuring consistency in the imaging and measurement parameters utilized. This should help confirm these findings and the HL-60 cell-line's use as a model, provide more statistically significance to the data, and keep said data consistent with the actual biology of the cells.

Ultimately, the measurement of nuclear circulatory as a way to quantify changes in nuclear morphology is a promising method that has the capability to be applied to other research in cellular biology, as well as furthering research in neutrophil nuclear dynamics. Nuclear circularity as a metric has already been utilized to showcase differences in nuclear morphology between spindle cell melanoma cells and desmoplastic melanoma cells, two different sub-types of skin cancer, and therefore provide an added distinction to these two conditions to help with diagnosis (40). Considering this and the findings of this thesis, it is likely that circularity measurements could be an aid to a wide range of research which involve differences in nuclear morphology between different cell-types or changes induced by cells reacting to stimuli.

Nuclear circularity was utilized as a metric for tracking dynamics in nuclear morphology for differentiation and activation of ATRA and DMF dHL-60s. NOX and NE activity are not just required for PMA-induced NET formation as is known by the field, but also PMA-induced nuclear morphological change, while MPO and PAD4 are not. Additionally, PAD4 is required for both A23187-induced NETosis and nuclear morphological change. This method of observing changes in nuclear morphology could be utilized to ascertain what other known NETosis pathway proteins also play a role in the nuclear

morphological changes brought on by activation. For example, it is known that PMA activates PKCα and that PKCζ activates PAD4 (6, 19). An experiment inhibiting these PKC isoforms and observing the effect on stimulation induced changes in circularity of dHL-60s could demonstrate if, as early aspects of the activation pathway, they also contribute to the delobing of the nuclei. Inhibition of other PKC isoforms could also be done to observe whether any other isoforms that are not involved with NETosis are involved the part of the activation pathway that involves changes in nuclear morphology. There is also still the question of what proteins or mechanisms are directly causing these changes in nuclear morphology. As it is easier to generate knockouts for HL-60s than primary neutrophils, genetic manipulation of the cell-line as a model could be performed, and circularity used as a metric to observe what other genes and proteins are required for these changes in morphology. However, genes and proteins that might affect the delobulation of neutrophils might also affect the attainment of lobes during differentiation. For example, as previous work in the Murre lab has shown that LBR knockout prevents differentiation induced change in nuclear morphology (31). Attempting an LBR knockout in HL-60s will most likely prevent successful change into the differentiated nuclear shape, so testing for how LBR knockout would affect stimulation-induced nuclear shape changes would be difficult. One possible knockout that has a higher likelihood of succeeding is an MPO knockout. As it has been noted that complete-deficiency of MPO has a different effect on the NET formation aspect of the neutrophil activation pathway than MPO inhibition (39), an MPO knockout could affect changes in nuclear morphology while inhibition fails to.

Studies into how change in nuclear morphology affects the chromatin organization of the cell could also be considered. HiC could be performed on stimulated dHL-60s that were treated with inhibitors of different proteins thought to affect activation at later times in the pathway that also affect nuclear morphology (for example NE or PAD4), and comparing these chromosomal interactions to the interactions seen in properly stimulated cells and unstimulated cells could elucidate what interactions brought on by activation are associated with change in nuclear morphology and what are associated with activation alone. If there are no differences between the stimulated inhibitor treated cells and the unstimulated cells, this could indicate that inhibiting the activation pathway to the extent that the nuclei fail to change shape inhibits

the cells from being activated entirely, as it is unknown if blocking these nuclear morphology dynamics completely blocks activation or not.

Ultimately, this research provides a solid foundation for future research into neutrophil nuclear morphology dynamics.

APPENDIX

Table 1. Wilcoxon rank sum test p-value data concerning the difference in nuclei circularity.

Experiment Description	Wilcoxon Test Samples	p-value
HL-60 ATRA and DMF Differentiation	HL-60 vs ATRA dHL-60	4.01147E-05
	HL-60 vs DMF dHL-60	3.64723E-05
ATRA dHL-60 Stimulation with PMA or A23187	Unstimulated vs PMA	0.001331392
	Unstimulated vs A23187	0.8686247
DMF dHL-60 Stimulation with PMA or A23187	Unstimulated vs PMA	0.9787377
	Unstimulated vs A23187	0.1092104
	Pooled Unstimulated vs A23187	2.43E-09
ATRA dHL-60 PMA Stimulation with DPI Treatment	Unstimulated DMSO vs Unstimulated DPI	0.6124615
	Unstimulated DMSO vs PMA DMSO	0.09159635
	PMA DMSO vs PMA DPI	0.6388396
ATRA dHL-60 PMA Stimulation with ABAH Treatment	Unstimulated DMSO vs Unstimulated ABAH	0.858777
	Unstimulated DMSO vs PMA DMSO	7.75E-05
	PMA DMSO vs PMA ABAH	0.4839058

Table 1. Wilcoxon rank sum test p-value data concerning the difference in nuclei circularity, continued.

Experiment Description	Wilcoxon Test Samples	P-Value
ATRA dHL-60 PMA Stimulation with NEi Treatment	Unstimulated No NEi vs Unstimulated NEi	0.5366388
	Unstimulated No NEi vs PMA NEi	0.0754911
	PMA No NEi vs PMA NEi	0.1029237
DMF dHL-60 A23187 Stimulation with GSK484 Treatment	Unstimulated DMSO vs Unstimulated GSK484	0.007465923
	Unstimulated DMSO vs A23187 DMSO	2.47E-11
	A23187 DMSO vs A23187 GSK484	4.98E-11
	Unstimulated GSK484 vs A23187 DMSO	2.47E-11
ATRA dHL-60 PMA Stimulation with GSK484 Treatment	Unstimulated DMSO vs Unstimulated GSK484	0.03043051
	Unstimulated DMSO vs PMA DMSO	0.8757896
	PMA DMSO vs PMA GSK484	4.67E-08

REFERENCES

1. Amulic B, Cazalet C, Hayes GL, Metzler KD, and Zychlinsky A. Neutrophil function: from mechanisms to disease. *Annual Review of Immunology*. 2012;30:459–489.

2. Brinkmann V, and Zychlinsky A. Neutrophil extracellular traps: Is immunity the second function of chromatin? *The Journal of Cell Biology*. 2012;198(5):773-783. doi:10.1083/jcb.201203170.

3. Hong CW. Current Understanding in Neutrophil Differentiation and Heterogeneity. *Immune Network*. 2017;17(5):298–306.

4. Mayadas TN, Cullere X, and Lowell CA. The Multifaceted Functions of Neutrophils. *Annual Review of Pathology*. 2014;9:181–218.

5. Branzk N, and Papayannopoulos V. Molecular mechanisms regulating NETosis in infection and disease. *Seminars in Immunopathology*. 2013;35(4):513-530. doi:10.1007/s00281-013-0384-6.

6. Steinberg SF. Structural Basis of Protein Kinase C Isoform Function. *Physiological Reviews*. 2008;88(4):1341-1378. doi:10.1152/physrev.00034.2007.

7. Hakkim A, Fuchs TA, Martinez NE, Hess S, Prinz H, Zychlinsky A, and Waldmann H. Activation of the Raf-MEK-ERK pathway is required for neutrophil extracellular trap formation. *Nature Chemical Biology*. 2011;7(2):75-7. doi:10.1038/nchembio.496.

8. Gupta AK, Giaglis S, Hasler P, and Hahn S. Efficient Neutrophil Extracellular Trap Induction Requires Mobilization of Both Intracellular and Extracellular Calcium Pools and Is Modulated by Cyclosporine A. *PLoS ONE*. 2014;9(5):e97088. doi:10.1371/journal.pone.0097088

9. Kenny EF, Herzig A, Krüger R, Muth A, Mondal S, Thompson PR, Brinkmann V, Bernuth HV, and Zychlinsky A. Diverse stimuli engage different neutrophil extracellular trap pathways. Brakhage AA, ed. *eLife*. 2017;6:e24437. doi:10.7554/eLife.24437.

10. Fuchs TA, Abed U, Goosmann C, Hurwitz R, Schulze I, Wahn V, Weinrauch Y, Brinkmann V, and Zychlinsky A. Novel cell death program leads to neutrophil extracellular traps. *The Journal of Cell Biology*. 2007;176(2):231-241. doi:10.1083/jcb.200606027.

11. Rochael NC, Guimarães-Costa AB, Nascimento MTC, DeSouza-Vieira TS, Oliveira MP, Garcia e Souza LF, Oliveira MF, and Saraiva EM. Classical ROS-dependent and early/rapid ROS-independent release of Neutrophil Extracellular Traps triggered by Leishmania parasites. Scientific Reports. 2015;5:18302. doi:10.1038/srep18302.

12. Cross AR, and Jones OT. The effect of the inhibitor diphenylene iodonium on the superoxide-generating system of neutrophils. Specific labelling of a component polypeptide of the oxidase. *Biochemical Journal*. 1986;237(1):111-116.

13. Metzler KD, Goosmann C, Lubojemska A, Zychlinsky A, and Papayannopoulos V. A Myeloperoxidase-Containing Complex Regulates Neutrophil Elastase Release and Actin Dynamics during NETosis. *Cell Reports*. 2014;8(3):883-96. doi:10.1016/j.celrep.2014.06.044.

14. Papayannopoulos V, Metzler KD, Hakkim A, and Zychlinsky A. Neutrophil elastase and myeloperoxidase regulate the formation of neutrophil extracellular traps. *The Journal of Cell Biology*. 2010;191(3):677-691. doi:10.1083/jcb.201006052.

15. Kettle AJ, Gedye CA, and Winterbourn CC. Mechanism of inactivation of myeloperoxidase by 4-aminobenzoic acid hydrazide. *Biochemical Journal*. 1997;321(Pt 2):503-508.

16. Macdonald SJ, Dowle MD, Harrison LA, Shah P, Johnson MR, Inglis GG, Clarke GD, Smith RA, Humphreys D, Molloy CR, Amour A, Dixon M, Murkitt G, Godward RE, Padfield T, Skarzynski T, Singh OM, Kumar KA, Fleetwood G, Hodgson ST, Hardy GW, and Finch H. The discovery of a potent, intracellular, orally bioavailable, long duration inhibitor of human neutrophil elastase--GW311616A a development candidate. *Bioorganic & Medicinal Chemistry Letters.* 2001;11(7):895-8. doi:10.1016/S0960-894X(01)00078-6

17. Brinkmann V, Reichard U, Goosmann C, Fauler B, Uhlemann Y, Weiss DS, Weinrauch Y, and Zychlinsky A. Neutrophil Extracellular Traps Kill Bacteria. *Science*. 2004;303(5663):1532-1535. doi:10.1126/science.1092385

18. Balasubramanian SV, Sikdar SK, and Easwaran KRK. Bilayers containing calcium ionophore A23187 form channels. *Biochemical and Biophysical Research Communications*. 1992;189(2):1038-1042. doi:10.1016/0006-291X(92)92308-K.

19. Neeli I, and Radic M. Opposition between PKC isoforms regulates histone deimination and neutrophil extracellular chromatin release. *Frontiers in Immunology*. 2013;4:38. doi:10.3389/fimmu.2013.00038.

20. Wang Y, Li M, Stadler S, Correll S, Li P, Wang D, Hayama R, Leonelli L, Han H, Grigoryev SA, Allis CD, and Coonrod SA. Histone hypercitrullination mediates chromatin decondensation and neutrophil extracellular trap formation. *The Journal of Cell Biology*. 2009;184(2):205-213. doi:10.1083/jcb.200806072.

21. Lewis HD, Liddle J, Coote JE, Atkinson SJ, Barker MD, Bax BD, Bicker KL, Bingham RP, Campbell M, Chen YH, Chung CW, Craggs PD, Davis RP, Eberhard D, Joberty G, Lind KE5, Locke K, Maller C, Martinod K, Patten C, Polyakova O, Rise CE, Rüdiger M, Sheppard RJ, Slade DJ, Thomas P, Thorpe J, Yao G, Drewes G, Wagner DD, Thompson PR, Prinjha RK, and Wilson DM. Inhibition of PAD4 activity is sufficient to disrupt mouse and human NET formation. *Nature Chemical Biology*. 2015;11(3):189-191. doi:10.1038/nchembio.1735.

22. Fuhrmann J, Clancy KW, and Thompson PR. Chemical Biology of Protein Arginine Modifications in Epigenetic Regulation. *Chemical Reviews*. 2015;115(11):5413-5461. doi:10.1021/acs.chemrev.5b00003.

23. Guiducci E, Lemberg C, Küng N, Schraner E, Theocharides APA, and LeibundGut-Landmann S. Candida albicans-Induced NETosis Is Independent of Peptidylarginine Deiminase 4. *Frontiers in Immunology*. 2018;9:1573. doi:10.3389/fimmu.2018.01573.

24. Ruiz-Velasco M, and Zaugg JB. Structure meets function**:** How chromatin organisation conveys functionality. *Current Opinion in Systems Biology.* 2017;1:129-136. doi:10.1016/j.coisb.2017.01.003.

25. Rudan MV, Barrington C, Henderson S, Ernst C, Odom DT, Tanay A, and Hadjur S. Comparative Hi-C Reveals that CTCF Underlies Evolution of Chromosomal Domain Architecture. *Cell Reports*. 2015;10(8):1297-1309. doi:10.1016/j.celrep.2015.02.004.

26. Neems DS, Garza-Gongora AG, Smith ED, and Kosak ST. Domain-derived myogenic genome topology. *Proceedings of the National Academy of Sciences*. 2016;113(12):E1691-E1700. doi:10.1073/pnas.1521826113

27. Skinner BM, and Johnson EEP. Nuclear morphologies: their diversity and functional relevance. *Chromosoma*. 2017;126(2):195-212. doi:10.1007/s00412-016-0614-5.

28. Carvalho LO, Aquino EN, Neves AC, and Fontes W. The Neutrophil Nucleus and Its Role in Neutrophilic Function. *Journal of Cellular Biochemistry*. 2015;116(9):1831-6. doi:10.1002/jcb.25124.

29. Gaines P, Tien CW, Olins AL, Olins DE, Shultz LD, Carney L, and Berliner N. Mouse neutrophils lacking lamin B receptor expression exhibit aberrant development and lack critical functional responses. *Experimental Hematology*. 2008;36(8):965-976. doi:10.1016/j.exphem.2008.04.006.

30. Zhang X, Kluger Y, Nakayama Y, Poddar R, Whitney C, DeTora A, Weissman SM, and Newburger PE. Gene expression in mature neutrophils: early responses to inflammatory stimuli. *Journal of Leukocyte Biology*. 2004;75(2):358-72. doi:10.1189/jlb.0903412

31. Zhu Y, Gong K, Denholtz M, Chandra V, Kamps MP, Alber F, and Murre C. Comprehensive characterization of neutrophil genome topology. *Genes & Development*. 2017;31(2):141-153. doi:10.1101/gad.293910.116.

32. Rao SSP, Huntley MH, Durand NC, Stamenova EK, Bochkov ID, Robinson JT, Sanborn AL, Machol I, Omer AD, Lander ES, and Aiden EL. A 3D Map of the Human Genome at Kilobase Resolution Reveals Principles of Chromatin Looping. *Cell*. 2014;159(7):1665-1680. doi:10.1016/j.cell.2014.11.021

33. Van Roozendaal KE, Darling D, and Farzaneh F. DMSO and retinoic acid induce HL-60 differentiation by different but converging pathways. *Experimental Cell Research*. 1990;190(1):137-40. doi:10.1016/0014-4827(90)90155-4

34. Wang J, Fong CC, Tzang CH, Xiao P, Han R, and Yang M. Gene expression analysis of human promyelocytic leukemia HL-60 cell differentiation and cytotoxicity induced by natural and synthetic retinoids. *Life Sciences*. 2009;84(17-18):576-83. doi:10.1016/j.lfs.2009.02.001

35. Manda-Handzlik A, Bystrzycka W, Wachowska M, Sieczkowska S, Stelmaszczyk-Emmel A, Demkow U, and Ciepiela O. The influence of agents differentiating HL-60 cells toward granulocyte-like cells on their ability to release neutrophil extracellular traps. *Immunology Cell Biology*. 2018;96:413-425. doi:10.1111/imcb.12015

36. Rueden CT, Schindelin J, Hiner MC, DeZonia BE, Walter AE, Arena ET, and Eliceiri KW. ImageJ2: ImageJ for the next generation of scientific image data. *BMC Bioinformatics*. 2017;18:529. doi:10.1186/s12859-017-1934-z.

37. Preibisch S, Saalfeld S, and Tomancak P. Globally optimal stitching of tiled 3D microscopic image acquisitions. *Bioinformatics*. 2009;25(11):1463-1465. doi:10.1093/bioinformatics/btp184.

38. RStudio Team. RStudio: Integrated Development for R. Boston, MA: RStudio, Inc; 2016. http://www.rstudio.com/.

39. Metzler KD, Fuchs TA, Nauseef WM, Reumaux D, Roesler J, Schulze I, Wahn V, Papayannopoulos V, and Zychlinsky A. Myeloperoxidase is required for neutrophil extracellular trap formation: implications for innate immunity. *Blood*. 2011;117(3):953-959. doi:10.1182/blood-2010-06-290171.

40. Schöchlin M, Weissinger SE, Brandes AR, Herrmann M, Möller P, and Lennerz JK. A nuclear circularity-based classifier for diagnostic distinction of desmoplastic from spindle cell melanoma in digitized histological images. *Journal of Pathology Informatics*. 2014;5:40. doi:10.4103/2153-3539.143335.